Mechanisms and effects of under-ice warming water in Ngoring Lake of Qinghai-Tibet Plateau

Mengxiao Wang [1,2], Lijuan Wen [1*], Zhaoguo Li [1], Matti Leppäranta [3], Victor Stepanenko [4,5], Yixin Zhao [1,2], Ruijia Niu [1,2], Liuyiyi Yang [1,2] and Georgiy Kirillin [6]

[1] Key Laboratory of Land Surface Process and Climate Change in Cold and Arid Regions, Northwest Institute of Eco-Environment and Resources, Chinese Academy of Sciences, 730000 Lanzhou, China

[2] University of Chinese Academy of Sciences, 10049 Beijing, China

[3] Institute of Atmospheric and Earth Sciences, University of Helsinki

[4] Research Computing Center, Lomonosov Moscow State University, Moscow, Russia

[5] Moscow Center for Fundamental and Applied Mathematics, Moscow, Russia

[6] Department of Ecohydrology, Leibniz-Institute of Freshwater Ecology and Inland Fisheries (IGB), Berlin, Germany

*Correspondence to: Lijuan Wen (wlj@lzb.ac.cn)

Abstract The seasonal ice cover in lakes of the Qinghai-Tibet Plateau is a transient and vulnerable part of the cryosphere, whose characteristics depend on the regional climate: strong solar radiation in the context of the dry and cold environment. We use the first under-ice temperature observations from the largest Tibetan freshwater lake Ngoring and a one-dimensional lake model to quantify the mechanism of solar thermal accumulation under ice, which relies on the ice optical properties and weather conditions, as well as the effect of the accumulated heat on the land-atmosphere heat exchange after the ice break-up. The model was able to realistically simulate the feature of Ngoring Lake thermal regime: the "summer-like" temperature stratification with temperatures exceeding the maximum density point of 3.98 °C across the bulk of the water column. A series of sensitivity experiments revealed solar radiation was the major source of under-ice warming and demonstrated that the warming phenomenon was highly sensitive to the optical properties of ice. The heat accumulated under ice contributed to the heat release from the lake to the atmosphere for 1-2 months after ice-off, increasing the upward sensible and latent surface heat fluxes on average by ~50 W m^{-2} and ~80 W m^{-2}, respectively. Therefore, the delayed effect of heat release on the land-atmosphere interaction requires an adequate representation in regional climate

modeling of the Qinghai-Tibet Plateau and other lake-rich alpine areas.

1 Introduction

Seasonal lake ice is a part of the cryosphere, gaining recent attention from researchers due to its sensitivity to climate change (Kirillin et al., 2012; Sharma et al., 2020). The duration of ice cover affects the stability and vertical mixing of lakes, as well as the lake-atmosphere matter and energy exchange (Rösner et al., 2012; Efremova et al., 2013; Ramp et al., 2015). Ice cover regulates lake biochemical indicators, such as the concentration of dissolved oxygen, nitrogen, and phosphorus, changing the biochemical reaction rate and affecting the water quality and distribution of aquatic organisms (Weitere et al., 2010; Dokulil, 2013; Li et al., 2015a; Hardenbicker et al., 2016). Shortening of the ice season has been observed worldwide (Sharma et al., 2019; Dauginis and Brown 2021) and attributed to anthropogenic warming (Grant et al., 2021). Future climate predictions indicated the accelerated reduction of seasonal lake ice, especially pronounced in the lake-rich Arctic regions (Brown and Duguay 2011). Global assessment of seasonal lake ice changes requires quantification of the major heat sources and sinks on seasonal to climatic time scales. While the major prerequisite for the ice cover development is sufficient long season with air temperature below the freezing point of water, the heat budget of ice-covered lakes varies with latitude and altitude, depending strongly on the available solar radiation, the latter being the major source of heat for under-ice lake water (Kirillin et al., 2012). During the polar night in the Arctic and temperate lakes covered by snow, the solar heating is minor and the bottom sediment is the main heat source (Winter I according to Kirillin et al., 2012); at later stages of the ice season (Winter II), as the snow melts, solar radiation becomes to the main heat source governing thermal stratification and mixing under ice and the melting process at the ice base (Kirillin et al., 2018, 2020). Further, lakes with seasonal ice cover can be divided into cryomictic and cryostratified according to their maximum depth, surface area, and wind speed (Yang et al., 2021). In dry and cold areas with little snow, winter II can occupy the entire ice-covered period (Kirillin et al., 2012), making solar radiation to be the major factor affecting the lake ice regime. The situation is relevant to the alpine lakes.

In particular, the largest alpine lake system of the Qinghai-Tibet Plateau (TP), the highest plateau on Earth with an average altitude of 4000-5000 m ensures a high amount of solar radiation and low winter precipitation. The TP is covered by more than 1400 lakes with an area larger than 1 km^2, and the total lake area is more than 5×10^4 km^2, accounting for 57.2 % of that in China (Wan et al., 2016; Zhang et al., 2019). Recent

studies reported the first observations from ice-covered Tibetan lakes, indicating the major role of solar radiation in their thermal regime (Wang et al., 2021). Water temperatures in Lakes Bangong Co and Nam Co constantly increased during the ice-covered period, with a stronger increase in shallower Bangong Co (Lazhu et al., 2021). Observations in meromictic Dagze Co Lake demonstrated stable temperatures in the early ice-covered period start warming only in the late ice-covered period, conditioned by the high water salinity (Wang et al., 2014; Lazhu et al., 2021). Salinity has a strong influence on the temperature and mixing regime of all three abovementioned lakes, by altering their density stratification and vertical heat transport. Among freshwater lakes in the TP, Ngoring Lake is the largest one (Kirillin et al. 2017; Wen et al. 2022). Kirillin et al. (2021) found strong solar radiation under ice cover heating the entire lake water column to the maximum freshwater density temperature (~3.98 °C, T_{md}) more than a month before the ice breakup—the situation never found in lowland freshwater lakes. As a result, strong heat release from water to the ice base turned into the major factor governing the ice melt, with the water temperature under ice achieving 6 °C. This radiation-dominated regime, differing dramatically from the typical heat budget known from earlier studies on ice-covered lakes, does not fall under the framework of the Winter I/Winter II classification, nor can be characterized in terms of cryomictic/cryostratified conditions. Quantification of the resulting heat balance and thermal stratification characteristic of alpine conditions is the subject of the present study.

Due to the harsh environment of the TP and difficulties in collecting field observations, numerical models are often used to investigate phenomena and mechanisms of TP lakes. At present, the widely used lake models are the FLake model and the lake scheme coupled in the CLM (Community Land Model), CoLM (Common Land Model), and WRF (Weather Research and Forecasting Model) (Lazhu et al., 2016; Wen et al., 2016; Fang et al., 2017; Dai et al., 2018; Huang et al., 2019; Song et al., 2020; Wu et al., 2021). However, for computational efficiency, winter dynamics in these highly-parameterized lake models are represented in a rather simplified way, lacking the detailed mechanisms of heating by radiation and resulting vertical heat transports across the water column (Lazhu et al., 2016; Wen et al., 2016; Huang et al., 2019). As an alternative, we adopt for this study a "classical" two-equation turbulence modeling approach proving its reliability in decades of studies on the environmental turbulent fluid dynamics. The one-dimensional model LAKE implements the approach in application to lake dynamics and was applied previously to different lakes (Stepanenko et al., 2011, 2016; Guseva et al., 2016). We combine modeling with in situ observations from Ngoring Lake, data on weather forcing and remote sensing to: (i) test the ability of a one-dimensional lake model LAKE to simulate temperature and stratification

driven by intense solar heating in ice-covered Lake Ngoring; (ii) conduct series of sensitivity experiments aimed at revealing the role of meteorological forcing and ice optical properties in lake temperature and mixing regime; and (iii) reveal the effects of temperature distribution before ice breakup on lake heat storage and lake- atmosphere heat transfer.

2 Study area and data

2.1 Study area

Ngoring Lake (34.76-35.08º N, 97.53-97.90º E, Fig. 1) is located in the western valley of Maduo County on the eastern TP, with an average lake surface elevation of 4274 m a.s.l. It is the largest freshwater lake in the Yellow River source region with a salinity of about 0.27 g kg^{-1} (Shen et al., 2012). It has a surface area of 610 km^2, a maximum depth of 32 m, and an average depth of 17 m. The pH is 8.49 and there are very few fish in the lake. Aquatic plants grow only in the riparian area. The lake thermally stratifies in summer and is covered by ice from late November or early December to late April (Wen et al., 2016). According to observational data from 1953 to 2016 at Maduo station (34.9º N, 98.2º E) of the China Meteorological Administration, the average annual precipitation was 322.4 mm, mostly concentrated from May to September. The average annual air temperature was -3.53 ºC. The maximum air temperature was 24.3 ºC occurred on July 20, 2006, and the minimum air temperature was -48.1 ºC occurred on January 2, 1978.
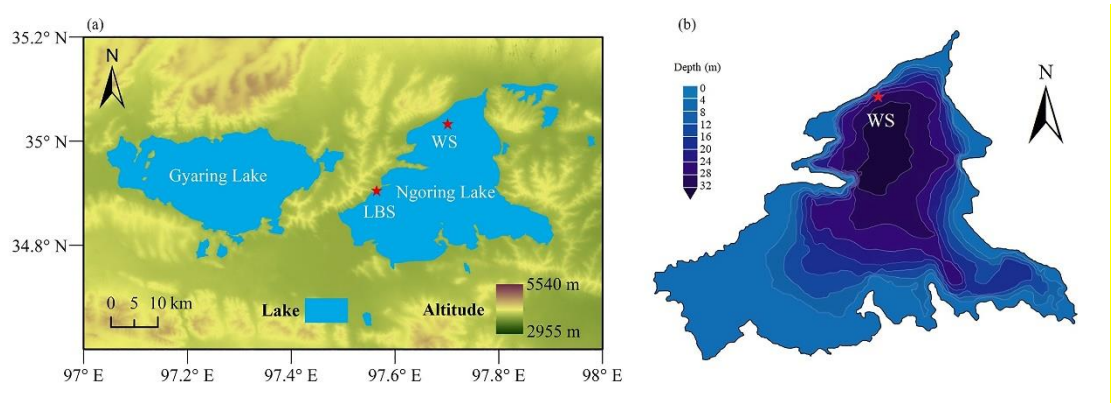

Figure 1. (a) Location and (b) bathymetry of Ngoring Lake. (b) is adapted from Kirillin et al., 2021. The pentagrams denote the lake border station (LBS) and water temperature measurement site (WS).

2.2 Data

2.2.1 Observational data: LBS station and WS site

The long-term automatic lake border station (LBS, 34.91º N, 97.55º E, Fig. 1) was installed in October 2012, with an altitude of 4282 m a.s.l., providing meteorological forcing data: wind speed at 10 m, air temperature, specific humidity and air pressure at 2 m, downward shortwave (SR) and longwave radiation (LR) at 1.5 m from September 2015 to September 2016 (Li et al., 2020). The detailed information about site configuration and measured quantities are referred to in Li et al. (2015b) and Wen et al. (2016). The precipitation was obtained from the daily value data set (V3.0) at Maduo station of Chinese surface climate data (http://data.cma.cn).

The water temperature measurement site (WS, 35.03º N, 97.70º E, Fig. 1) was located in the northern of Ngoring Lake, where the total water depth was about 26.5 m. The multi-layer water temperature observation system consisted of 16 self-recording RBR SOLO water temperature probes with a precision of 0.01 ℃. The sampling distance and time intervals were 1 m and 10 minutes, respectively.

2.2.2 MODIS lake surface temperature

The 8-day L3 global lake surface temperature product (MYD11C2) was derived from the data of Moderate Resolution Imaging Spectroradiometer (MODIS) and was used to evaluate the simulated results. MODIS offers long-term daily global coverage data with high spatial resolution. This product provides an 8-day combined radiative surface temperature at approximately 10:30 and 22:30 LT (local time), which is the satellite transit time. The resolution is 0.05º latitude/longitude (5600 m at the equator) for Climate Modeling Grid (CMG) (https://ladsweb.nascom.nasa.gov/search) (Wan et al., 2004).

2.2.3 ERA5-Land data

ERA5-Land is produced as an enhanced global dataset for the land component of the fifth generation of European ReAnalysis (ERA5) by the European Centre for Medium-Range Weather Forecasts (ECMWF), framed within the Copernicus Climate Change Service (C3S) of the European Commission. It is available for ERA5-Land hourly record for about 40 years from 1981 to the present. Expediently, ERA5-Land has an enhanced horizontal resolution of 9 km (~0.08º) compared to ERA5 (31 km) and ERA-Interim (80 km) (https://cds.climate.copernicus.eu/cdsapp#!/dataset/reanalysis-

era5-land?tab=form) (Hersbach et al., 2020; Muñoz-Sabater et al., 2021).

ERA5-Land data is applied for a comparative analysis of warming mechanisms and thermal conditions in Tibetan ice-covered lakes against those in the Arctic. The reanalysis forcing data for the geographical position 69.05º N, 20.83º E was adopted as "typical" arctic weather conditions. Northern Fennoscandia is covered by several lakes characterized by the longest ice-covered period in Western Europe. The largest of these lakes, Kilpisjärvi, has a similar morphometrical feature to Ngoring (average depth 19.5 m, maximum depth 57 m, surface area 37 km^2). The lake has been intensively studied in the last decades (Kirillin et al., 2015, 2018; Leppäranta et al., 2017, 2019). Its under-ice water temperature remained stable during winter from 1992 to 1993 (Tolonen, 1998). In the following, model experiments forced by the ERA5 weather data (1992-1993) for the Arctic refer to "Kilpisjärvi" runs.

3 Methods

3.1 LAKE model

The one-dimensional model LAKE, simulating thermodynamic, hydrodynamic, and biogeochemical processes, is used to solve the horizontally averaged transfer of gases, heat, salts, and momentum in an enclosed water body (Stepanenko et al., 2011, 2016). The vertical heat diffusion is simulated, and the penetration of solar radiation into the water ice, snow, and bottom sediments layers (Heiskanen et al., 2015; Cao et al., 2020) is taken into account. The exchange between the water and the inclined bottom is modeled explicitly because the model equations have been averaged over horizontal sections of the water body. The 2nd order κ-ε parametrization of turbulence is applied (Stepanenko et al., 2016).

3.1.1 Heat transfer in water body

The water temperature is calculated according to the one-dimensional thermal diffusion equation:

$$c_w \rho_w \frac{\partial T_w}{\partial t} = -c_w \rho_w \frac{1}{A} \int_{\Gamma_A} T_w (u_h \cdot n) dl + \frac{1}{Ah^2} \frac{\partial}{\partial \xi} \left(A_w K_T \frac{\partial T_w}{\partial \xi} \right) - \frac{1}{Ah} \frac{\partial AS}{\partial \xi} +$$

$$\frac{1}{Ah} \frac{\partial A}{\partial \xi} \left[S_b(\xi) + F_{iz,b}(\xi) \right] + \frac{dh}{dt} \frac{\xi}{h} \frac{\partial T_w}{\partial \xi} , \qquad (1)$$

where c_w is water specific heat, ρ_w is water density, T_w is water temperature, $h(t)$ is lake depth, t is time, $\xi = z/h$ is a normalized vertical coordinate ($z \in [0, h]$), $z = 0$ is located at the free water surface of the lake, S is downward shortwave radiation, A_w is

the z-dependent cross-sectional area of water, K_T is thermal diffusivity coefficient equal to the sum of molecular and turbulent diffusivities, $S_b(\xi)$ is shortwave radiation flux, $F_{iz,b}$ is soil heat flux at the level z, n is an outer normal vector to the boundary Γ_A of the horizontal cross-section A and u_h is horizontal vector in water (Stepanenko et al., 2016; Guseva et al., 2016).

3.1.2 Heat transfer in ice cover

==When the air temperature decreases below 0 °C and the surface water temperature drops to the freezing point, the initial ice cover forms. When the net radiation of the lake is positive, the ice melts continuously until the ice thickness declines to zero. The general heat conduction equation in ice cover follows the equation:==

$$c_i \rho_i \frac{\partial T_i}{\partial t} = c_i \rho_i \frac{\xi}{h_i} \frac{dh_i}{dt} \frac{\partial T_i}{\partial \xi} - c_i \rho_i \frac{1}{h_i} \frac{dh_{i0}}{dt} \frac{\partial T_i}{\partial \xi} - \frac{1}{h_i} \frac{\partial S}{\partial \xi} + \frac{1}{A_i h_i^2} \frac{\partial}{\partial \xi} \left(A_i \lambda_i \frac{\partial T_i}{\partial \xi} \right) + \frac{1}{A_i h_i} \frac{\partial A_i}{\partial \xi} F_{T,b} -$$

$$L \rho_i \frac{dp}{dt} \ , \qquad (2)$$

where c_i is ice specific heat, ρ_i is ice density, T_i is ice temperature, λ_i is ice thermal conductivity, h_i is ice thickness, $\frac{dh_{i0}}{dt}$ is the increment of ice thickness on its surface, $F_{T,b}$ is the heat flux at the ice-sediment boundary, A_i is the z-dependent cross-sectional area of the ice cover determined by the basin morphometry, L is the latent heat of water and p is ice porosity (Stepanenko et al., 2019). The last term to the right-hand side presents heat of phase transition of salty water in ice pores.

The penetration of solar radiation into the medium is calculated using the Beer-Lambert law (Stepanenko and Lykossov, 2005; Stepanenko et al., 2019):

$$S(\xi) = S(0) \exp(-a_e h \xi) \ , \qquad (3)$$

where a_e is the medium extinction coefficient. To solve the temperature in Eq. (1 & 2), it is necessary to specify the top and bottom boundary conditions and provide the method to calculate the heat flux at each depth z. The atmospheric turbulent heat flux schemes are based on the Monin-Obukhov similarity theory (Stepanenko et al., 2016).

When the lake is covered by ice, the temperatures of the bottom layer of ice and the top layer of water are equal and fixed to the melting/freezing point temperature (Stepanenko et al., 2019), which is calculated by the following formula:

$$T_{mp} = - C * \left| \partial T_{mp} / \partial C \right| \ , \qquad (4)$$

where T_{mp} is the melting/freezing point temperature (°C), C is salinity at the water-ice interface, $\left| \partial T_{mp} / \partial C \right| = 66.7$ °C is assumed constant.

Based on the study by Leppäranta (2014), the albedo regulates the surface energy

budget, and the extinction coefficient controls the vertical distribution of radiation energy in the medium. In the LAKE model, the albedo of water (A_w) is 0.06, and the snow extinction coefficient (E_s) decreases with increased snow density. Snow accumulation in the Ngoring Lake area is almost zero. Therefore, only A_i, E_i, and E_w are analyzed in this study. Version 2.3 called LAKE2.3 is used in this article.

3.2 Methods to evaluate the model accuracy

The indexes to evaluate accuracy of the model are the root mean square error ($RMSE$), $BIAS$, and correlation coefficient (CC):

$$RMSE = \sqrt{\frac{1}{n}\sum_{j=0}^{n}\left(m_j - o_j\right)^2} \ , \qquad (5)$$

$$BIAS = \bar{m} - \bar{o} \ , \qquad (6)$$

$$CC = \frac{\text{Cov}(M,O)}{\sqrt{\text{Var}(M)\,\text{Var}(O)}} \ , \qquad (7)$$

where m_j and o_j represent the simulations and observations. $\bar{m}$ and $\bar{o}$ are the corresponding average values. $\text{Var}(M)$ and $\text{Var}(O)$ are the variances of observed and simulated values, respectively. $\text{Cov}(M,O)$ is the covariances.

3.3 Calculation method of heat storage

The heat storage evolution in water is calculated by the following formulation:

$$Q = c_w \rho_w \sum_{k=1}^{n} T_k \Delta z_k \ , \qquad (8)$$

where c_w = 4192 J kg^{-1} K^{-1} and ρ_w = 10^3 kg m^{-3}, n is the layer number, Δz_k is depth interval between two successive layers and T_k (K) is the average temperature in layer k (Nordbo et al., 2011; Gan and Liu, 2020).

4 Characteristic analysis of water temperature and local climate in two lakes

4.1 Characteristics of water temperature

It is pointed out that the under-ice water temperature from 2015 to 2016 in Ngoring Lake rose continuously during the entire ice-covered period according to observations (Wang et al., 2021; Kirillin et al., 2021). In November, the lake mixed evenly with slight oscillation (<1 °C between 2 m and 22 m) and water temperature decreased gradually

until the lowest point of 0.47 °C at 2 m on December 12, the lake froze up completely (Fig. 2a). Meanwhile, the air temperature at 2 m fell to -7.79 °C. Ngoring Lake is mostly covered only by bare ice in winter due to drought, less precipitation and snow. In the early ice-covered phase (from December 12 to March 7), the whole lake mixed completely because solar radiation penetrated ice and heated the upper water, which was warm (< T_{md}), heavy and sinking (Fig. 2b) (Kirillin et al., 2012). In parallel, water temperature continued to warm until reached T_{md} on March 7 (Fig. 2a).

In the late ice-covered stage (from March 7 to April 18), the lake stratified. On the one hand, owing to solar radiation strengthened, on the other hand, since radiation absorption of water decayed with depth based on the Beer-Lambert law. Water temperature increased at the rate of 0.052 °C d^{-1} in the layers from 2 m to 6 m, which was more rapid than the early stage of 0.035 °C d^{-1}. On April 18, the ice melted entirely as well water temperature rose to 5.83 °C at 2 m while remaining at T_{md} below 9 m. After that, full mixing took place rapidly because the lake warmed gaining heat from the sun and atmosphere as a result of ice breaking up (Fig. 2b).
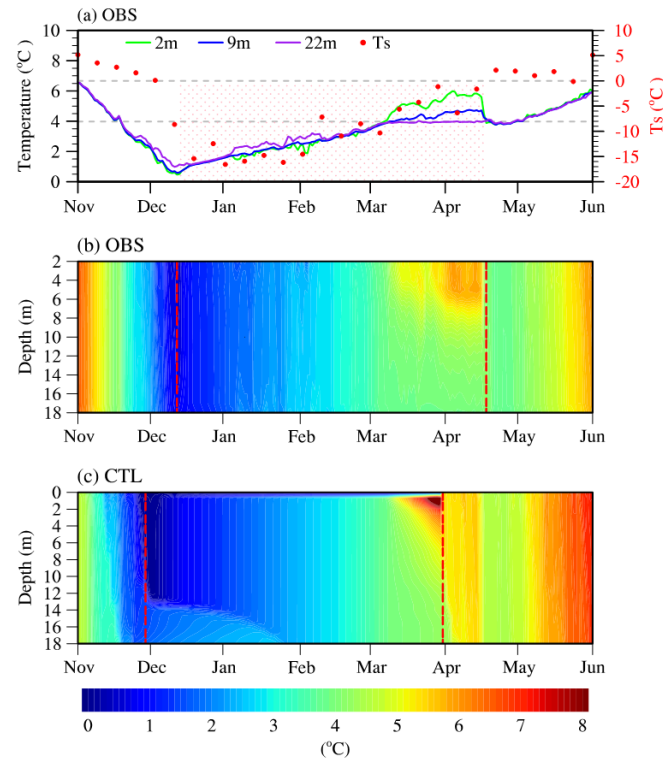

Figure 2. (a) The daily average water temperature observations of Ngoring Lake at the surface (Ts), 2 m, 9 m, and 22 m from November 1, 2015 to June 1, 2016. Ts is MODIS lake surface temperature. The gray reference lines denote 3.98 °C and 0 °C, respectively. The pink shaded area denotes ice-covered period. The water temperature profile (b) observed and (c) simulated in CTL. The ice-covered period is represented between the two red dashed lines.

4.2 Local climate: Tibet vs. Kilpisjärvi

The daily averages of meteorological variables between Tibet and Kilpisjärvi were shown in Fig. 3, the ranges and averages of that during the ice-covered period (from December 12 to April 18 based on Ngoring Lake) were compared (Table 1). The average differences in air temperature, specific humidity, and downward LR were -0.42 °C, -0.38 g kg^{-1}, and 41.9 W m^{-2}, respectively. The wind speed of Tibet was 1.7 times that of Kilpisjärvi, and the downward SR in Tibet of 199.41 W m^{-2} was stronger than in Kilpisjärvi of 40.46 W m^{-2}. The precipitation was a multiple of 0.037 in Tibet than that in Kilpisjärvi.

On the whole, there were few differences in air temperature, specific humidity, and downward LR in the two regions. Nevertheless, there was much lower precipitation, much higher downward SR and wind speed in Tibet. Surface pressure was not considered in this study since the little effect on water temperature.
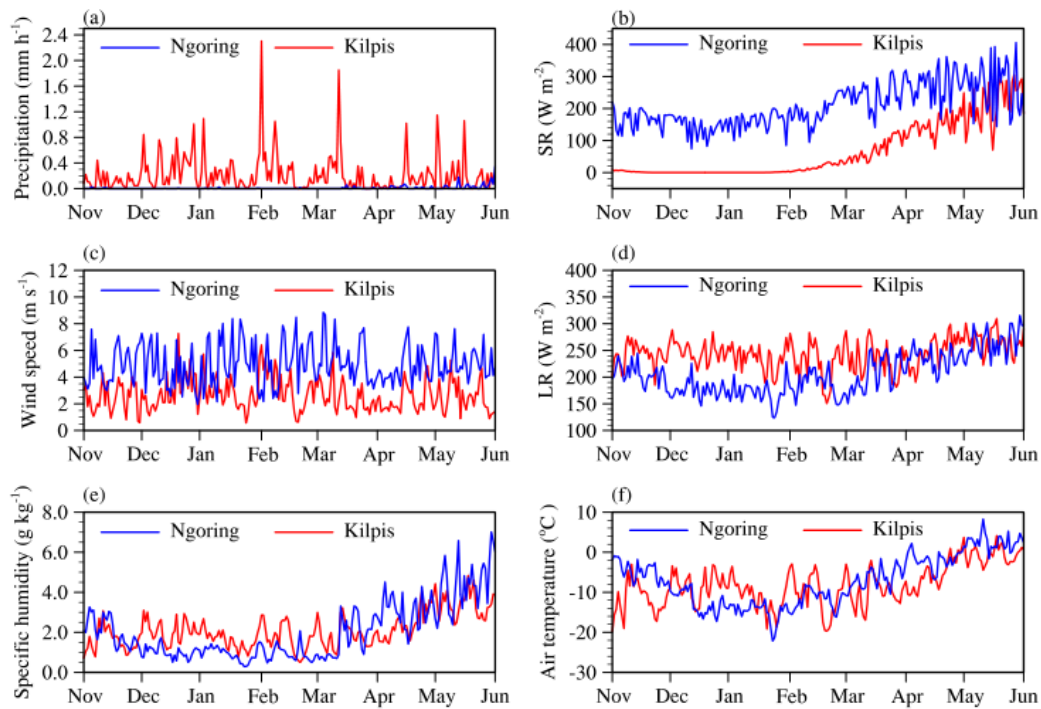

Figure 3. Comparison of daily average values of the meteorological variables for Tibet from 2015 to 2016 and for Kilpisjärvi from 1992 to 1993. (a) precipitation, (b) downward SR, (c) wind speed, (d) downward LR, (e) specific humidity, and (f) air temperature. The "Ngoring" represents the Tibet region and the "Kilpis" represents Kilpisjärvi region.

Table 1. Ranges and averages of the meteorological variables of Tibet (2015-2016) compared with Kilpisjärvi (1992-1993) during the ice-covered period (12.12-4.18).

Meteorologic variables	Tibet		Kilpisjärvi	
	Range	Average	Range	Average
Precipitation (mm h^{-1})	< 0.072	0.0044	< 1.15	0.12
Downward SR (W m^{-2})	73.98-356.29	199.41	< 186.84	40.46
Wind speed (m s^{-1})	1.95-8.85	4.93	0.56-7.28	2.83
Downward LR (W m^{-2})	123.92-271.60	191.73	150.61-289.59	233.62
Specific humidity (g kg^{-1})	0.29-4.52	1.40	0.50-3.23	1.78
Air temperature (℃)	-22.16-2.24	-10.25	-19.69-2.01	-9.83

5 Simulation setup

To reveal the mechanism of water temperature rising during ice-covered period in Ngoring Lake and its further influences, one control simulation (CTL) and 27 sensitivity simulations (SIM) depending on CTL were set in this study (Table 2).

5.1 Setup in CTL

The depth was set as 26.5 m, measured at the WS point, and divided vertically into 35 layers. The simulation period was from September 2015 to September 2016. The initial vertical profile of water temperature, mixed layer, and the bottom temperature were set following the observations (Fig. 2b). The albedos of snow and ice and the extinction coefficients of ice and water were set as $A_s = 0.7$, $A_i = 0.25$, $E_i = 2.5$ m^{-1}, and $E_w = 0.15$ m^{-1} based on previous investigations (Lei et al., 2011; Li et al., 2018, 2020;

323 Shang et al., 2018). The input driving meteorological variables were air pressure, wind
324 speed, specific humidity, air temperature, precipitation, downward SR, and LR. The
325 forcing data and model run interval was 30 minutes and 15 seconds respectively.

326

327 **5.2 Setup in SIM**

328   To explore the influence of a single meteorological variable, SIM_* simulations
329 were set up. The symbol * is SR, Precip, LR, U, Tair, or q in Kilpisjärvi. These scenarios
330 were quite artificial because these variables are closely correlated. Despite that, these
331 sensitivity simulations can shed light on the influence of local climate on lake
332 temperature evolution during ice-covered period.
333   To discuss the effect of main physical parameters, SIM_# simulations were set up,
334 the sign # represented the values of A_i, E_i, or E_w. SIM_E* (* equal to 1, 2, or 3) is set
335 for exploring the effects of three different initial water temperature profiles before ice
336 breakup on the lake heat storage and heat fluxes.

337

338 **Table 2.** Names, explanations, and amounts of all experiments.

Experiment name	Experiment explanation	Amount
CTL	Control simulation	1
SIM_* (* represents meteorological variables)	The simulation when the * variable is replaced by that of Kilpisjärvi.	6
SIM_# (# represents values of A_i, E_i or E_w)	The simulation when the corresponding physical variable is equal to #, respectively.	18
SIM_E* (* represents 1, 2, and 3)	The simulation when using three different initial temperature profiles before ice melting based on CTL.	3

339

340 **6 Simulation results**

341 **6.1 Model validation**
342   The simulations in CTL were relatively consistent with the observations (Fig. 2b,c),

even though the whole ice season advanced by about 15 days than observed. Water temperature was a little higher in CTL than that in the observations from mid-March to late May. The deviation was greater in the deep water. The simulated temperature warmed faster and higher by 1 ℃ than the observed value after ice melted.

The results were evaluated by calculating *RMSE, BIAS, CC* between simulated and observed water temperature at the lake surface (Ts), 2 m, 9 m and 22 m (Fig. 4). The *CC* in each layer was equal to even greater than 0.95, and the *CC* in 2 m and 9 m are as high as 0.98, even though *RMSE* and *BIAS* of lake surface were 3.25 ℃ and 1.42 ℃, respectively. The Ts *RMSE* was largely due to the uncertainty of MODIS lake surface temperature (Donlon et al., 2002; Tavares et al., 2019). The *BIAS* absolute values in the internal lake were less than 0.01 ℃, and *RMSE* was less than 0.95 ℃. More important, the under-ice temperature warming phenomenon was reproduced reasonably.
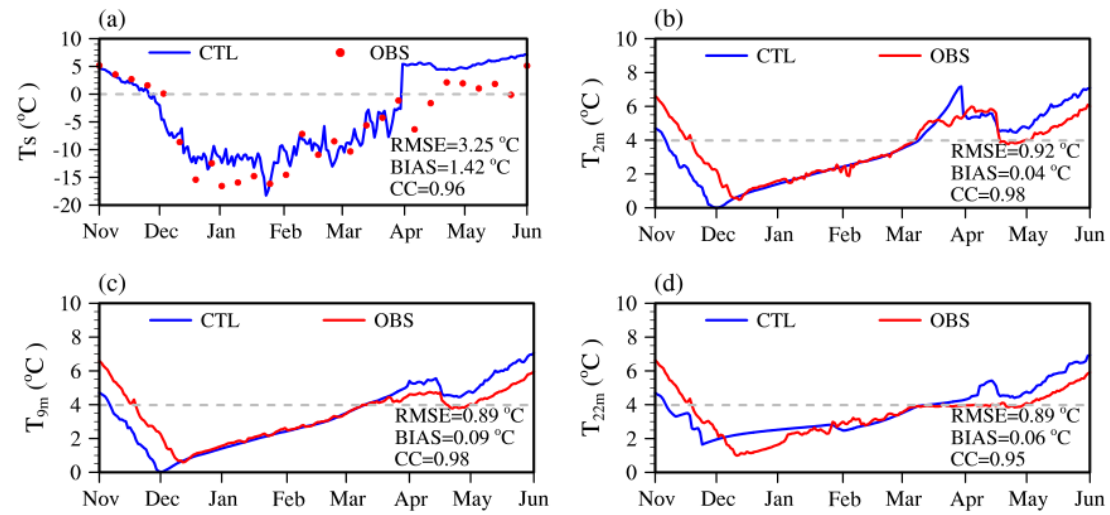

Figure 4. The daily average water temperature observed and simulated in CTL of (a) the surface (Ts), (b) 2 m, (c) 9 m, (d) 22 m in Ngoring Lake from November 2015 to June 2016. The dotted line represents T_{md} 3.98 ℃.

6.2 Influences of local climate on water temperature

To explore the influences of local climate on water temperature, six simulations SIM_* (* represents 6 meteorological variables, Table 2) were designed. The 3 m water temperature was typically selected to analyze since water temperature at different depths varied consistently over time.

SIM_SR was the simulation when the Kilpisjärvi downward SR was substituted for that in Tibet. During the ice-covered period, the downward SR difference between CTL (199.41 W m^{-2}) and SIM_SR (40.46 W m^{-2}) was 158.95 W m^{-2}. In the sensitivity simulation SIM_SR, the 3 m water temperature was stable keeping in the range of 0-

0.1 °C (Fig. 5a). The ice formation date was earlier and the ice-breaking date delayed, which led to the growth of the whole ice season. The mixed layer depth increased (Fig. 5d). Consequently, the strong downward SR on the TP generated the under-ice water warming in Ngoring Lake.

In the simulation SIM_Precip, the Tibet precipitation was replaced by that in Kilpisjärvi. In the sensitivity experiment SIM_Precip, the 3 m water temperature fixed, then increased but did not exceed T_{md} in the early ice cover stage (Fig. 5a). The stratification and temperature maximum center disappeared in late March, and the lake was fully mixed (Fig. 2c,5g). Because the average precipitation in SIM_Precip (0.12 mm h^{-1}) was approximately 30 times larger than that in CTL (0.0044 mm h^{-1}) during ice-covered period, more solar radiation was reflected and absorbed by snow due to more snowfall accumulation. Thus, the high precipitation damped the water temperature rise.

In SIM_LR simulation, the downward LR in Kilpisjärvi superseded that in Tibet. The average downward LR was 233.62 W m^{-2} in SIM_LR, which was stronger than that in CTL (191.73 W m^{-2}) during ice-covered period. The 3 m water temperature still warmed as well the complete ice melting time of late February was ahead. The heat was transferred from lake to atmosphere because of lower air temperature after ice breakup. The water temperature underwent a cooling process (2 °C) until reaching a new equilibrium with atmosphere (Fig. 5b). Compared with the CTL, water mixing in the ice-covered period was more uniform, the stratification in late March was weakened, and the temperature maximum center advanced about 15 days (Fig. 5e).

In SIM_U simulation, the wind speed of Kilpisjärvi was substituted for that of Tibet. The wind speed in SIM_U (2.83 m s^{-1}) was weaker than that in CTL (4.93 m s^{-1}) for the ice cover period. In the sensitivity experiment SIM_U, the 3 m water temperature kept rising, but it was about 3 °C higher than that in CTL during the whole simulation period (Fig. 5b). Due to the decrease in wind speed, the mixed layer depth was reduced, and the lake stratification was more stable (Fig. 5h).

In SIM_T_{air} simulation, the air temperature of Kilpisjärvi was replaced by that of Tibet. The average air temperature difference between SIM_T_{air} (-9.83 °C) and CTL (-10.25 °C) was negligible (0.42 °C). In the sensitivity experiment SIM_T_{air}, the water temperature decreased more quickly, and in late October, the lake froze no longer releasing heat into atmosphere. The lake stratification was enhanced, and the water temperature maximum center was ahead about 10 days (Fig. 5c,f).

In SIM_q simulation, the specific humidity of Kilpisjärvi was substituted for Tibet. The difference in specific humidity between SIM_q and CTL was 0.38 g kg^{-1} during

ice-covered period. In the sensitivity experiment SIM_q, the simulations were coincidental to that in CTL, and thus the specific humidity had little effect on the water temperature (Figs. 5c,i).

In conclusion, the stronger downward SR and lower precipitation in TP played positive roles in the water temperature warming during the ice-covered period in Ngoring Lake. Less downward LR, lower air temperature, and larger wind speed did not change the warming trend but affected the warming amplitude and rate. Specific humidity had no significant influence.
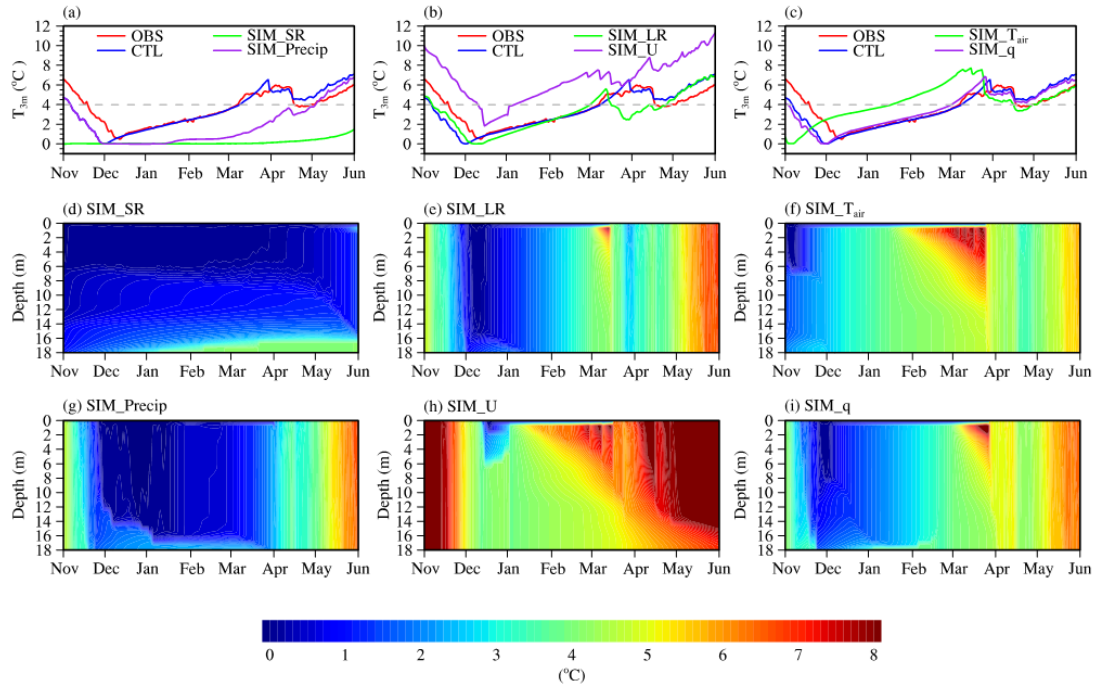

Figure 5. The simulated 3 m daily average water temperature in (a) (d) SIM_SR, (a) (g) SIM_Precip, (b) (e) SIM_LR, (b) (h) SIM_U, (c) (f) SIM_T_{air}, (c) (i) SIM_q sensitivity experiments from November 2015 to June 2016 are compared with the CTL and the observation, and the change of vertical stratification is shown. The dotted line represents 3.98 °C.

6.3 Influences of main physical parameters on water temperature

The radiation transfer, which depended on the albedo and extinction coefficient, played a decisive role in the water temperature. Only influences of A_i, E_i, and E_w on water temperature simulation were discussed with sensitivity experiments due to less snow in Tibet. According to previous observations, A_i has observed on TP was mostly less than 0.12, and the albedo of clear blue ice was only 0.075 (Li et al., 2018). The range of A_i without snow cover was set as 0.1-0.8 with an interval of 0.1 in SIM_A_i

427   experiments.

428   E_i has not been observed on TP, but surveys in Finnish lakes show that the value of

429   bare ice varies between 1-4 m^{-1}, while the value of snow-covered ice can reach 5 m^{-1}

430   (Lei et al., 2011). In SIM_E_i simulations, E_i was equal to 1-5 m^{-1} with an interval of 1

431   m^{-1}.

432   For the E_w, Zolfaghari et al. (2017) found that the FLake model is particularly

433   sensitive at $E_w \leq 0.5 \ m^{-1}$. Shang et al. (2018) observed that E_i varies from 0.11 to 0.67

434   m^{-1} in a few TP lakes. Therefore, the sensitivity simulations SIM_E_w were designed in

435   which the E_w varied from 0.1 to 0.5 m^{-1} with an increment step of 0.1 m^{-1}. The

436   experimental settings are shown in Table 3.

437

438   **Table 3.** Numerical sensitivity simulations of parameters affecting the radiative transfer.

Parameter	CTL	SIM_A_i	SIM_E_i	SIM_E_w
A_i	0.25	0.1/0.2/0.3/0.4/0.5 /0.6/0.7/0.8	0.25	0.25
E_i (m^{-1})	2.5	2.5	1.0/2.0/3.0/4.0 /5.0	2.5
E_w (m^{-1})	0.15	0.15	0.15	0.1/0.2/0.3/0.4 /0.5

439

440   In the SIM_A_i sensitivity experiment, the 3 m water temperature decreased

441   approximately 1 °C when ice albedo increased by 0.1. When the albedo grew to 0.80,

442   the water temperature warming decreased from 4 °C to 2 °C. The increase of ice albedo

443   did not affect the ice formation date but remarkably delayed the ice melting time,

444   accordingly prolonging the ice-covered period. When the albedo increased from 0.1 to

445   0.8, the ice-covered period was extended for 15-30 days for every 0.1 increase (Fig. 6a).

446   In the sensitivity experiment SIM_E_i, the ice extinction coefficient changes did not

447   all make a continuous rising in water temperature, but the 3 m water temperature

448   decreased by 1-2 °C when ice extinction coefficient increased by 1 m^{-1} (Fig. 6b). The

449   ice absorbed more heat, and the less heat entered the lake water under ice due to the

450   larger ice extinction coefficient.

451   To further discuss influences of A_i and E_i on lake temperature during ice-covered

452   period. The period was divided into two stages Period-A and Period-B in CTL, SIM_A_i.

Period-A ranged from freezing point to T_{md}, Period-B ranged from T_{md} to maximum temperature (T_m). The duration of Period-A is longer than that of Period-B, and the temperature heating rate in Period-B (~ 0.1 °C d^{-1}) was 2.5 times greater than that of Period-A (~ 0.04 °C d^{-1}). The reason was that lake completely covered by ice, and the inner lake evenly mixed in Period-A, while the ice thickness decreased and the radiation absorbed by the ice decreased in Period-B. The upper layer absorbed more heat than the deeper layer, and the upper water temperature increased rapidly. When A_i and E_i increased, the heating rate decreased and the duration increased in Period-A, the T_max decreased, the heating rate and duration fluctuate in Period-B. When $A_i \geq 0.6$, the heating rate during ice-covered period decreases and did not rise to T_{md}.

In the SIM_Ew sensitivity experiment, the water extinction coefficient had just a little influence on the winter water temperature, 3 m water temperature decreased with the increase of Ew (Fig. 6c). When only the extinction coefficient of water changed, the solar radiation entering the water through the ice is unchanged, and so the heat storage of the lake was unaffected. It's just that the heat distribution in the vertical direction is changed. The higher the extinction coefficient of water, the more heat was absorbed by the surface layer and the less heat reached the deep layer. The phenomenon that the 3 m water temperature decreases with the extinction coefficient increasing becomes more and more obvious in the later stage of ice melting.
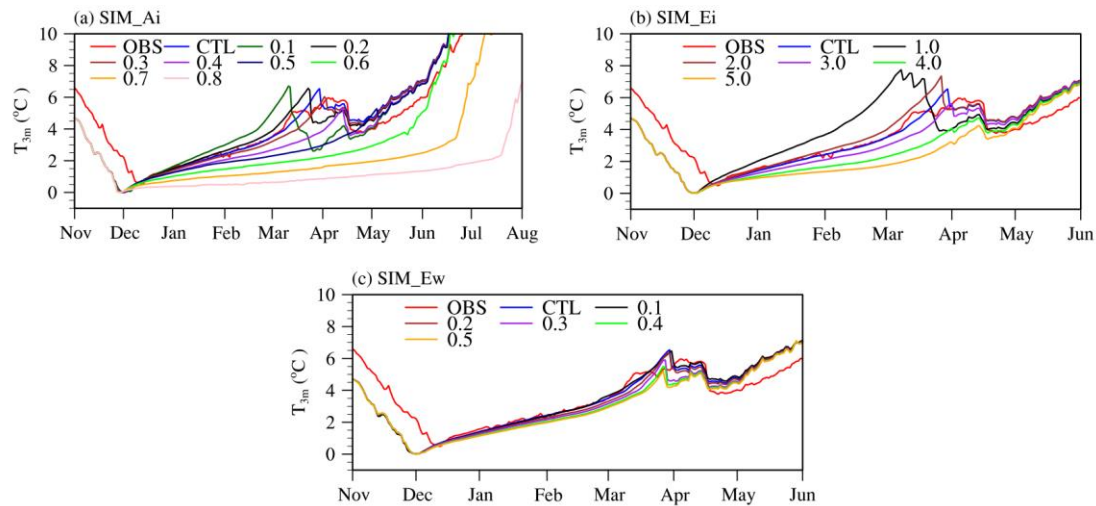

Figure 6. Comparison of the 3m simulated daily average water temperature with the observed value under different (a) A_i, (b) E_i, (c) E_w.

6.4 Influences of water temperature on lake-atmosphere exchange

The thermal conditions in an ice-covered lake just before ice melting have a significant influence on the air-lake energy exchange. To analyze the effects of lake

temperature characteristics on the atmosphere at ice melting, three experiments – SIM_E1, SIM_E2, and SIM_E3 (Table 1) – were set up based on the CTL and the observed lake temperature profile on March 25, 2016, 5 days before ice completely melted (Fig. 7a). The characteristics of the initial water temperature profile were:

- SIM_E1. The stratification was weak, the first layer temperature was at the melting point, and, from the second layer down, the water temperature was set as 2 ℃ corresponding to Bangong Co (Wang et al., 2014).
- SIM_E2. The lake was strongly stratified. The first layer was at the melting point, and the temperature increased linearly reaching T_{md} at the bottom, corresponding to Valkea-Kotinen Lake (Bai et al., 2016).
- SIM_E3. The temperature of the first layer was at the melting point, and the temperature gradually increased with the depth from the second layer to the middle layer, and the temperature in the middle layer increased to T_{md} corresponding to Thrush Lake (Fang and Stefan, 1996).

In CTL, the first layer temperature equal to the freezeing/melting point, and the second layer reached the maximum temperature on March 25. The temperature became lower with the deeper layer, until the temperature reached T_{md}.

With the different initial temperature profiles, the heat storage was different after ice breakup, and the difference persisted for about two months (Fig. 7b). In CTL, from March 30 to March 31 when ice melted completely, the lake heat storage ranged from 30893.02 MJ m^{-2} to 30874.51 MJ m^{-2}, and the heat released was 18.51 MJ m^{-2}. In the three experiments, from April 1 to April 2 when ice melted completely, the lake heat storage changed from 30657.51 MJ m^{-2} to 30651.67 MJ m^{-2} in SIM_E1, from 30781.07 MJ m^{-2} to 30769.91 MJ m^{-2} in SIM_E2, and from 30833.28 MJ m^{-2} to 30822.42 MJ m^{-2} in SIM_E3, and the heat release was 5.84 MJ m^{-2}, 11.16 MJ m^{-2}, and 10.86 MJ m^{-2}, respectively (Fig. 7b).

The heat released was in the form of sensible heat and latent heat, accounting for 0.060% (CTL), 0.019% (SIM_E1), 0.036% (SIM_E2), and 0.035% (SIM_E3) of the ice-covered heat storage, respectively. As the initial lake temperature profiles were different before ice complete melting, the ice melted earlier and faster with the higher lake temperature. The lake heat storage increased from March 25 to May 24, and the heat release rate was different under different circumstances. After late May, the heat balance between the lake and the atmosphere was the same, and so the heat storage basically stayed equally after that.
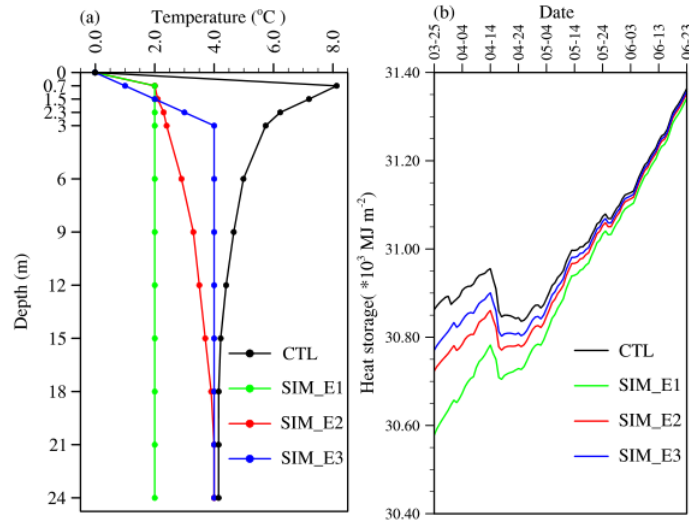
Figure 7. (a) The initial water temperature profiles in the model are set on March 25, 2016, and the corresponding daily average (b) lake heat storage is simulated. SIM_E1, SIM_E2, and SIM_E3 are three different sensitivity simulations.

The lake surface temperature also affected the sensible and latent heat release, whose differences were calculated between CTL and the three experimental simulations (Fig. 8). The influence of different initial water temperature profiles started on March 31, that is, when the ice had melted completely in CTL, and when the sensible and latent differences between CTL and three experimental simulations were less than 0.1 W m^{-2} for three consecutive days, we judged that the influence had ended. The maximum differences of the sensible heat (51.0 W m^{-2}) and latent heat (76.7 W m^{-2}) between SIM_E1 and CTL appeared on March 31 and ended on June 12 and 30, respectively (Fig. 8a). In SIM_E2 the corresponding numbers were 51.4 W m^{-2} (March 31 to June 5) for sensible heat and 81.7 W m^{-2} (April 1 to June 17) for latent heat (Fig. 8b), and in SIM_E3 they were 51.5 W m^{-2} (March 31 to May 23) for sensible heat and 86.0 W m^{-2} (April 1 to June 5) for latent heat (Fig. 8c). Compared with the three lake temperature experiments, the heating characteristics of Ngoring Lake made the heat release higher and faster during ice breakup. The duration of heat release difference was from 59 (to May 23) to 97 (to June 30) days, and for the latent heat release, the situation lasted about 12-18 days longer than for the sensible heat release.
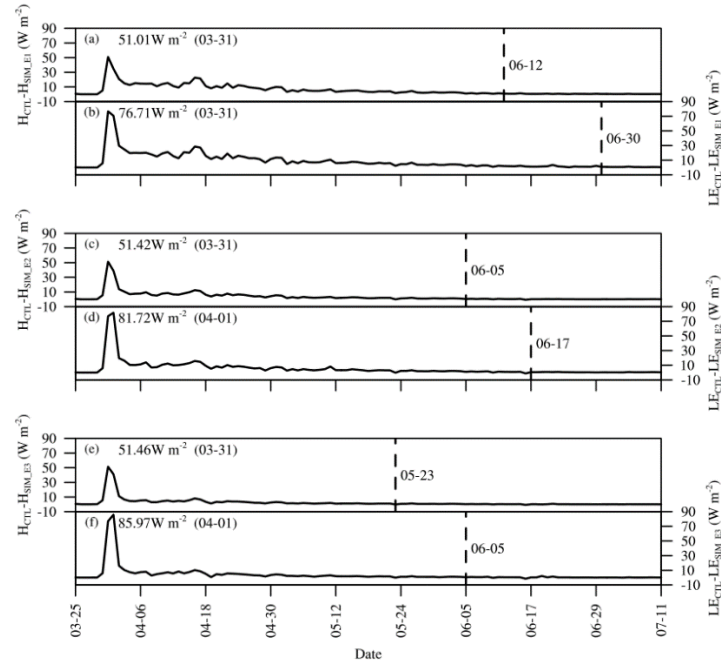
534

Figure 8. The daily average difference between the sensitivity sensible and latent heat and the CTL under three different initial water temperature profiles in SIM_E1, SIM_E2, and SIM_E3.

7 Conclusions

The analysis demonstrates a significant increase in lake temperature during the ice-covered period in Ngoring, the largest freshwater lake on the Tibetan Plateau (TP), with water temperatures exceeding the freshwater maximum density value T_{md}. The heating is governed by strong solar radiation, the factor differing alpine lakes on the TP from the low-altitude northern lakes with similar winter air temperature patterns. The one-dimensional lake model LAKE2.3 successfully captured the major mechanisms of warming and vertical thermal stratification during the ice-covered period. Compared with MODIS surface temperature data, the *BIAS*, *RMSE,* and *CC* were 1.42 °C, 3.25 °C, and 0.96, respectively. The absolute values of *BIAS* and *RMSE* were less than 0.1 °C and 1 °C in 2 m, 9 m, 14 m, and 22 m. The *CC* of simulated and observed water temperature at 2 m, 9 m, and 14 m were as high as 0.98, and the *CC* of simulated and observed water temperature at 22 m was 0.95.

Sensitivity simulations with perturbed local climate data confirmed the decisive role of subsurface solar radiation in the water temperature rise and demonstrated strong negative feedback with winter precipitation amount. The downward longwave radiation, air temperature, and wind speed had only a minor influence on the water temperature.

The warming rates and, as a result, the duration of the ice-covered period was

20

sensitive to the physical ice properties: ice albedo and light extinction coefficient both reduced the amount of the subsurface solar radiation. An increase in the albedo of ice reduced the rising trend of water temperature and prolonged the ice season. At the critical albedo of 0.6, the lake water warming decreased obviously and temperature remained stable no more than 3.98 ℃. The extinction coefficient of water had just a minor effect on water temperature under the ice.

An important consequence of the under-ice solar heat accumulation consisted in increased sensible and latent heat releases in the subsequent open-water phase. According to the model results, the effects on the surface fluxes of Ngoring Lake lasted for 59-97 days after the ice melt and increased the upward latent and sensible surface heat fluxes up to ~80 W m^{-2} and ~50 W m^{-2}, respectively. Herewith, the phenomenon of under-ice solar heating may have a significant effect on the land-atmosphere interaction on regional scales and has to be accounted for in coupled climate models.

Data availability. The daily precipitation data from Chinese surface stations are available for purchase from the China Meteorological Data Service Center (CMDC, http://data.cma.cn/en/). The MODIS LST product is available from National Aeronautics and Space Administration (NASA) (https://earthdata.nasa.gov/). ERA5-Land data is available with funding from the European Union's Copernicus Climate Change Service (https://cds.climate.copernicus.eu/). Lake temperature data of Ngoring Lake in 2015 and 2016 were uploaded to Zenodo by Georgiy Kirillin (http://doi.org/10.5281/zenodo.4750910). The weather observation data of Ngoring Lake can be obtained from the website (https://nimbus.igb-berlin.de/index.php/s/Moqxgn29DbNFyr8). The latest version of LAKE model source code is available at Zenodo: https://zenodo.org/record/6353238#.YjCSXi1eNTY .

Author contributions. MW and LW conceived the study. MW performed the modeling with contributions from VS, LW, and ZL. YZ, RN, and LY processed some data. MW, LW, ML, and GK analyzed the model output. MW wrote the paper, with contributions from all co-authors.

Competing interests. The authors declare that they have no conflict of interest.

References

Bai, Q. X., Li, R. L., Li, Z. J., Leppäranta, M., Arvola, L. and Li, M.: Time-series analyses of water temperature and dissolved oxygen concentration in Lake Valkea-Kotinen (Finland) during ice season, Ecol Inform, 36, 181-189, doi: 10.1016/j.ecoinf.2015.06.009, 2016.

Brown, L. C. and Duguay, C. R.: The fate of lake ice in the North American Arctic, The Cryosphere, 5, 869-892, doi: 10.5194/tc-5-869-2011, 2011.

Cao, X. W., Lu, P., Leppäranta M., Arvola L., Huotari J., Shi X. H., Li G. Y. and Li Z. J.: Solar radiation transfer for an ice-covered lake in the central Asian arid climate zone, Inland Waters, 11, 89-103, doi: 10.1080/20442041.2020.1790274, 2020.

Dai, Y. J., Wei, N., Huang, A. N., Zhu, S. G., Shangguan, W., Yuan, H., Zhang, S. P. and Liu, S. F.: The lake scheme of the Common Land Model and its performance evaluation (in Chinese), Chin Sci Bull, 63, 3002-3021, doi: 10.1360/n972018-00609, 2018.

Dauginis, A. A. and Brown, L. C.: Recent changes in Pan-Arctic sea ice, lake ice, and snow on/off timing, The Cryosphere, 15, 4781-4805, doi: 10.5194/tc-2021-52, 2021.

Dokulil, M. T.: Predicting summer surface water temperatures for large Austrian lakes in 2050 under climate change scenarios, Hydrobiologia, 731, 19-29, doi: 10.1007/s10750-013-1550-5, 2013.

Donlon, C. J., Minnett, P. J., Gentemann, C., Nightingale, T. J., Barton, I. J., Ward, B., and Murray, M. J.: Toward improved validation of satellite sea surface skin temperature measurements for climate research, J. Clim., 15, 353–369, doi: 10.1175/15200442(2002)015<0353:TIVOSS>2.0.CO;2, 2002.

Efremova, T., Palshin, N. and Zdorovennov, R.: Long-term characteristics of ice phenology in Karelian lakes, EST J EARTH SCI, 62, 33-41, doi: 10.3176/earth.2013.04, 2013.

Fang, N., Yang, K., Lazhu, Chen, Y. Y., Wang, J. B. and Zhu, L. P.: Research on the application of WRF-lake Modeling at Nam Co Lake on the Qinghai-Tibetan Plateau, Plateau Meteorology, 36, 610-618, doi: 10.7522/j.issn.1000-0534.2016.00038, 2017.

Fang, X. and Stefan, H. G.: Long-term lake water temperature and ice cover simulations/measurements, Cold Reg Sci Technol, 24, 289-304, 1996.

Gan, G. J. and Liu, Y. B.: Heat storage effect on evaporation estimates of China's largest freshwater lake, J. Geophys, 125, 1-14, doi: 10.1029/2019jd032334, 2020.

Grant, L.,Vanderkelen, I., Gudmundsson, L., Tan, Z., Perroud, M., Stepanenko, V., Debolskiy, A. V., Droppers, B., Janssen, A. B., Woolway, R. I., Choulga, M., Balsamo, G., Kirillin, G., Schewe, J., Zhao, F., Valle, I. V., Golub, M., Pierson, D., Marcé, R., Seneviratne, S. I. and Thiery, W.: Attribution of global lake systems change to anthropogenic forcing, Nat. Geosci., 14, 1-6, doi: 10.1038/s41561-021-00833-x, 2021.

Guseva, S., Stepanenko, V., Shurpali, N., Biasi, C., Marushchak, M. E. and Lind, S. E.:

Numerical simulation of methane emission from Subarctic Lake in Komi Republic (Russia), Geography, Environment, Sustainability, 9, 58-74, doi: 10.15356/2071-9388_02v09_2016_05, 2016.

Hardenbicker, P., Viergutz, C., Becker, A., Kirchesch, V., Nilson, E. and Fischer, H.: Water temperature increases in the river Rhine in response to climate change, Reg Environ Change, 17, 299-308, doi: 10.1007/s10113-016-1006-3, 2016.

Heiskanen, J. J., Mammarella, I., Ojala, A., Stepanenko, V., Erkkilä, K. M., Miettinen, H., Sandström, H., Eugster, W., Leppäranta, M., Järvinen, H., Vesala, T. and Nordbo, A.: Effects of water clarity on lake stratification and lake-atmosphere heat exchange, J. Geophys, 120, 7412-7428, doi: 10.1002/2014jd022938, 2015.

Hersbach, H., Bell, B., Berrisford, P., Hirahara, S., Horányi, A., Muñoz-Sabater, J., Nicolas, J., Peubey, C., Radu, R., Schepers, D., Simmons, A., Soci, C., Abdalla, S., Abellan, X., Balsamo, G., Bechtold, P., Biavati, G., Bidlot, J., Bonavita, M., Chiara, G., Dahlgren, P., Dee, D., Diamantakis, M., Dragani, R., Flemming, J., Forbes, R., Fuentes, M., Geer, A., Haimberger, L., Healy, S., Hogan, R. J., Hólm, E., Janisková, M., Keeley, S., Laloyaux, P., Lopez, P., Lupu, C., Radnoti, G., Rosnay, P., Rozum, I., Vamborg, F., Villaume, S. and Thépaut, J. N.: The ERA5 global reanalysis, Q J R Meteorol Soc, 146, 1999-2049, doi: 10.1002/qj.3803, 2020.

Huang, A. N., Lazhu, Wang, J. B., Dai, Y. J., Yang, K., Wei, N., Wen, L. J., Wu, Y., Zhu, X. Y., Zhang, X. D. and Cai, S. X.: Evaluating and improving the performance of three 1-D lake models in a large deep lake of the central Tibetan Plateau, J. Geophys, 124, 3143-3167, doi: 10.1029/2018JD029610, 2019.

Kirillin, G. B., Aslamov, I., Kozlov, V., Zdorovennov, R., and Granin, N.: Turbulence in the stratified boundary layer under ice: observations from Lake Baikal and a new similarity model, Hydrol. Earth Syst. Sci., 24, 1691-1708, doi: 10.5194/hess-24-1691-2020, 2020.

Kirillin, G. B., Aslamov, I., and Leppäranta, M.: Turbulent mixing and heat fluxes under lake ice: the role of seiche oscillations, Hydrol. Earth Syst. Sci., 22, 6493-6504, doi: 10.5194/hess-22-6493-2018, 2018.

Kirillin, G. B., Leppäranta, M., Terzhevik, A., Granin, N., Bernhardt, J., Engelhardt, C., Efremova, T., Golosov, S., Palshin, N., Sherstyankin, P., Zdorovennova, G. and Zdorovennov, R: Physics of seasonally ice-covered lakes: a review, Aquat Sci, 74, 659-682, doi: 10.1007/s00027-012-0279-y, 2012.

Kirillin, G. B., Wen, L. J. and Shatwell, T.: Seasonal thermal regime and climatic trends in lakes of the Tibetan highlands, Hydrol Earth Syst Sci, 21, 1895-1909, doi: 10.5194/hess-21-1895-2017, 2017.

Kirillin, G. B., Forrest, A. L., Graves, K. E., Fischer, A., Engelhardt, C. and Laval, B. E.: Axisymmetric circulation driven by marginal heating in ice-covered lakes, Geophys

Res Lett, 42, 2893-2900, doi: 10.1002/2014gl062180, 2015.

Kirillin, G. B., Shatwell, T. and Wen, L. J.: Ice-covered lakes of Tibetan Plateau as solar heat collectors, Geophys. Res. Lett., 48, 1-12, doi: 10.1029/2021gl093429, 2021.

Lazhu, Yang, K., Hou, J. Z., Wang, J. B., Lei, Y. B., Zhu, L. P., Chen, Y. Y., Wang, M. D. and He, X. G.: A new finding on the prevalence of rapid water warming durinig lake ice melting on the Tibetan Plateau, Sci. Bull., 66, 2358-2361, doi: 10.1016/j.scib.2021.07.022, 2021.

Lazhu, Yang, K., Wang, J. B., Lei, Y. B., Chen, Y. Y., Zhu, L. P., Ding, B. H. and Qin, J.: Quantifying evaporation and its decadal change for Lake Nam Co, central Tibetan Plateau, J. Geophys, 121, 7578-7591, doi: 10.1002/2015jd024523, 2016.

Lei, R. B., Leppäranta, M., Erm, A., Jaatinen, E. and Pärn, O.: Field investigations of apparent optical properties of ice cover in Finnish and Estonian lakes in winter 2009, EST J EARTH SCI, 60, 50-64, doi: 10.3176/earth.2011.1.05, 2011.

Leppäranta, M.: Freezing of lakes and the evolution of their ice cover, Germany: Springer Science & Business Media, 2014.

Leppäranta, M., Lindgren, E. and Shirasawa, K.: The heat budget of Lake Kilpisjärvi in the Arctic tundra, Hydrology Research, 48, 969-980, doi: 10.2166/nh.2016.171, 2017.

Leppäranta, M., Lindgren, E., Wen, L. J. and Kirillin, G.: Ice cover decay and heat balance in Lake Kilpisjärvi in Arctic tundra, J Limnol, 78, doi: 10.4081/jlimnol.2019.1879, 2019.

Li, G. C., Liu, Z. G., Zhang, M., Li, J., Pi, K., Xiong, Y. and Xu, J.: A preliminary study of effects of warming on the nutrients dynamic in sediment of hypereutrophic shallow lake, Acta Ecologica Sinica, 35, 4016-4025, doi: 10.5846/stxb201309102244, 2015a.

Li, Z. G., Ao, Y. H., Lyu, S. H., Lang, J. H., Wen, L. J., Stepanenko, V., Meng, X. H. and Zhao, L.: Investigation of the ice surface albedo in the Tibetan Plateau lakes based on the field observation and MODIS products, J Glaciol, 64, 506-516, doi: 10.1017/jog.2018.35, 2018.

Li, Z. G., Lyu, S. H., Ao, Y. H., Wen, L. J., Zhao, L. and Wang, S. Y.: Long-term energy flux and radiation balance observations over Lake Ngoring, Tibetan Plateau, Atmos Res, 155, 13-25, doi: 10.1016/j.atmosres.2014.11.019, 2015b.

Li, Z. G., Lyu, S. H., Wen, L. J., Zhao, L., Ao, Y. H. and Meng, X. H.: Study of freeze-thaw cycle and key radiation transfer parameters in a Tibetan Plateau lake using LAKE2.0 model and field observations, J Glaciol, 45, 1-16, doi: 10.1017/jog.2020.87, 2020.

Muñoz-Sabater, J., Dutra, E., Agustí-Panareda, A., Albergel, C., Arduini, G., Balsamo, G., Boussetta, S., Choulga, M., Harrigan, S., Hersbach, H., Martens, B., Miralles, D. G., Piles, M., Rodríguez-Fernández, N. J., Zsoter, E., Buontempo, C. and Thépaut, J.-N.: ERA5-Land: A state-of-the art global reanalysis dataset for land applications, Earth

Syst. Sci. Data, 1-50, doi: 10.5194/essd-2021-82, 2021.

Nordbo, A., Launiainen, S., Mammarella, I., Leppäranta, M., Huotari, J., Ojala, A. and Vesala, T.: Long-term energy flux measurements and energy balance over a small boreal lake using eddy covariance technique, J. Geophys, 116, 1-17, doi: 10.1029/2010jd014542, 2011.

Ramp, C., Delarue, J., Palsboll, P. J., Sears, R. and Hammond, P. S.: Adapting to a warmer ocean--seasonal shift of baleen whale movements over three decades, PLoS One, 10, 1-15, doi: 10.1371/journal.pone.0121374, 2015.

Rösner, R. R., Müller-Navarra, D. C. and Zorita, E.: Trend analysis of weekly temperatures and oxygen concentrations during summer stratification in Lake Plußsee: A long-term study, Limnol. Oceanogr., 57, 1479-1491, doi: 10.4319/lo.2012.57.5.1479, 2012.

Shang, Y. X., Song, K. S., Jiang, P., Ma, J. H., Wen, Z. D. and Zhao, Y.: Optical absorption properties and diffuse attenuation of photosynthetic active radiation for inland waters across the Tibetan Plateau, Journal of Lake Sciences, 30, 802-811, doi: 10. 18307 /2018. 0322, 2018.

Sharma, S., Blagrave, K., Magnuson, J. J., O'Reilly, C. M., Oliver, S., Batt, R. D., Magee, M. R., Winslow, L. and Woolway, R. I.: Widespread loss of lake ice around the Northern Hemisphere in a warming world, Nature Clim. Change., 9, 227-231, doi: 10.1038/s41558-018-0393-5, 2019.

Sharma, S., Meyer, M. F., Culpepper, J., Yang, X., Hampton, S., Berger, S. A., Brousil, M. R., Fradkin, S. C., Higgins, S. N., Jankowski, K. J., Kirillin, G.,Smits, A. P., Whitaker, E. C., Yousef, F. and Zhang, S.: Integrating Perspectives to Understand Lake Ice Dynamics in a Changing World, J Geophys Res-biogeo, 125, 1-18, doi: 10.1029/2020jg005799, 2020.

Shen, D. F., Li, S. J., Jiang, Y. J. and Chen, W.: Water environment characteristics and regional climate response of typical lakes in Yellow River headwater area, J. Arid Environ., 26, 91-97, doi: 10.13448/j.cnki.jalre.2012.07.030, 2012.

Song, X. Y., Wen, L. J., Li, M. S., Du, J., Su, D. S., Yin, S. C. and Lv, Z.: Comparative study on applicability of different lake models to typical lakes in Qinghai-Tibetan Plateau, Plateau Meteorology, 39, 213-225, doi: 10.7522/j.issn.1000-0534.2019.00102, 2020.

Stepanenko, V., Mammarella, I., Ojala, A., Miettinen, H., Lykosov, V. and Vesala, T.: LAKE 2.0: a model for temperature, methane, carbon dioxide and oxygen dynamics in lakes, Geosci Model Dev, 9, 1977-2006, doi: 10.5194/gmd-9-1977-2016, 2016.

Stepanenko, V. and Lykossov, V. N.: Numerical modeling of heat and moisture transfer processes in a system lake soil, Russ. Meteorol. Hydrol., 3, 95-104, doi: 2005.

Stepanenko, V., Machul'skaya, E. E., Glagolev, M. V. and Lykossov, V. N.: Numerical

modeling of methane emissions from lakes in the permafrost zone, IZV ATMOS OCEAN PHY+, 47, 252-264, doi: 10.1134/s0001433811020113, 2011.

Stepanenko, V., Repina, I. A., Ganbat, G. and Davaa, G.: Numerical simulation of ice cover of saline lakes, IZV ATMOS OCEAN PHY+, 55, 129-138, doi: 10.1134/s0001433819010092, 2019.

Tavares, M., Cunha, A., Motta-Marques, D., Ruhoff, A., Cavalcanti, J., Fragoso, C., Martín Bravo, J., Munar, A., Fan, F. and Rodrigues, L.: Comparison of methods to estimate Lake-Surface-Water temperature using Landsat 7 ETM+ and MODIS imagery: Case study of a large shallow subtropical lake in Southern Brazil, Water, 11, 1-21, doi: 10.3390/w11010168, 2019.

Tolonen, A.: Application of a bioenergetics model for analysis of growth and food consumption of subarctic whitefish Coregonus lavaretus (L.) in Lake Kilpisjärvi, Finnish Lapland, Hydrobiologia, 390, 153–169, doi: 10.1023/A:1003525008870, 1998.

Wan, W., Long, D., Hong, Y., Ma, Y. Z., Yuan, Y., Xiao, P. F., Duan, H. T., Han, Z. Y. and Gu, X. F.: A lake data set for the Tibetan Plateau from the 1960s, 2005, and 2014, Sci. Data, 3, 1-13, doi: 10.1038/sdata.2016.39, 2016.

Wan, Z., Zhang, Y., Zhang, Q. and Li, Z. L.: Quality assessment and validation of the MODIS global land surface temperature, Int J Remote Sens, 25, 261-274, doi: 10.1080/0143116031000116417, 2004.

Wang, M. D., Hou, J. Z. and Lei, Y. B.: Classification of Tibetan lakes based on variations in seasonal lake water temperature, Chinese Science Bulletin, 59, 4847-4855, doi: 10.1007/s11434-014-0588-8, 2014.

Wang, M. X., Wen, L. J., Li, Z. G. and Su, D. S.: Study on the warming characteristics during the ice-covered period of Ngoring Lake in the Qinghai-Xizang Plateau, Plateau Meteorology, 40, 965-976, doi: 10. 7522/j. issn. 1000-0534. 2020. 00112, 2021.

Weitere, M., Vohmann, A., Schulz, N., Linn, C., Dietrich, D. and Arndt, H.: Linking environmental warming to the fitness of the invasive clamCorbicula fluminea, Glob Chang Biol, 15, 2838-2851, doi: 10.1111/j.1365-2486.2009.01925.x, 2010.

Wen, L. J., Lyu, S. H., Kirillin, G., Li, Z. G. and Zhao, L.: Air–lake boundary layer and performance of a simple lake parameterization scheme over the Tibetan highlands, Tellus A, 68, 1-15, doi: 10.3402/tellusa.v68.31091, 2016.

Wen, L. J., Wang, C., Li, Z. G., Zhao, L., Lyu, S. H. and Chen, S. Q.: Thermal Responses of the Largest Freshwater Lake in the Tibetan Plateau and Its Nearby Saline Lake to Climate Change, Remote Sens, 14, 1-19, doi: 10.3390/rs14081774, 2022.

Wu, Y., Huang, A. N., Lazhu, Yang, X. Y., Qiu, B., Zhang, Z., Q. and Zhang X., D.: Numerical study of the thermal structure and circulation in a large and deep dimictic lake over Tibetan Plateau, J. Geophys, 126, 1-22, doi: 10.1029/2021jc017517, 2021.

Yang, B., Wells, M. G., McMeans, B. C., Dugan, H. A., Rusak, J. A., Weyhenmeyer, G.

784 A., Brentrup, J. A., Hrycik, A. R., Laas, A., Pilla, R. M., Austin, J. A., Blanchfield, P. J.,
785 Carey, C. C., Guzzo, M. M., Lottig, N. R., MacKay, M. D., Middel, T. A., Pierson, D.
786 C., Wang, J. and Young, J. D.: A new thermal categorization of ice-covered lakes,
787 Geophys. Res. Lett., 48, 1-11, doi: 10.1029/2020gl091374, 2021.
788 Zhang, G. Q., Luo, W., Chen, W. F. and Zheng, G. X.: A robust but variable lake
789 expansion on the Tibetan Plateau, Sci. Bull., 64, 1306-1309, doi:
790 10.1016/j.scib.2019.07.018, 2019.
791 Zolfaghari, K., Duguay, C. R. and Kheyrollah Pour, H.: Satellite-derived light
792 extinction coefficient and its impact on thermal structure simulations in a 1-D lake
793 model, Hydrol Earth Syst Sci, 1-36, doi: 10.5194/hess-2016-82, 2017.